Available online at www.sciencedirect.com

ScienceDirect

Ceramics International 39 (2013) 9207–9214

CERAMICS INTERNATIONAL

www.elsevier.com/locate/ceramint

Thiourea assisted one-pot easy synthesis of CdS/rGO composite by the wet chemical method: Structural, optical, and photocatalytic properties

Satheesh Kaveri[a], Lavanya Thirugnanam[b,c], Mrinal Dutta[b], Jayavel Ramasamy[a], Naoki Fukata[b,*]

[a]*Centre for Nanoscience and Technology, Anna University, Chennai 600025, India*
[b]*International Center for Materials Nanoarchitectonics (MANA), National Institute for Materials Science, 1-1 Namiki, Tsukuba 305-0044, Japan*
[c]*Department of Physics, Anna University, Chennai 600025, India*

Received 22 March 2013; received in revised form 7 May 2013; accepted 7 May 2013
Available online 14 May 2013

Abstract

We report on the synthesis of CdS/reduced graphene oxide (rGO) composite by a wet chemical method. Thiourea was used both as a sulfur source and as a reducing agent to convert graphene oxide to rGO. The structural and morphological confirmation for the reduction of graphene oxide and the formation of the CdS/rGO composite was demonstrated by X-ray diffractometry, Raman spectroscopy, Fourier transform infrared spectroscopy, transmission electron microscopy, and X-ray photoelectron spectroscopy analyses. Photoluminescence spectra of the composite exhibited a more efficient luminescence quenching in comparison with pure CdS nanoparticles. The composite demonstrated 99% photodegradation of methyl orange under UV irradiation, which is much superior than the photodegradation of methyl orange under similar conditions exhibited by CdS nanoparticles (72%).

Keywords: C. Optical properties; Wet chemical synthesis; CdS/rGO composite; Luminescence quenching; Photocatalytic properties

1. Introduction

Graphene, an sp^2 hybridized hexagonal arrangement of two dimensional honeycomb carbon lattice, has become the focus of recent research because of its extraordinary optical, thermal, electrical, and mechanical properties [1–4]. These properties hold great promise for technological applications in different areas such as nanoelectronics [5], sensors [6], photovoltaics [7], and energy storage materials [8,9]. Graphite oxide is the starting precursor for synthesizing graphene oxide (GO) sheets. GO has many oxygen-containing functional groups such as epoxy, hydroxyl, carbonyl, and carboxyl groups [10,11]. A growing interest has been evidenced in decorating the inorganic nanoparticles with graphene sheets to enhance their photocatalytic properties. The oxygen-containing functional groups of GO are very useful in attaching inorganic nanoparticles within graphene sheets. However, these functional groups act as scattering centers and alter the sp^2 in-plane bonding, thereby reducing the optical and electrical properties of graphene. Hence, regaining sp^2 aromaticity by reducing these functional groups becomes necessary to enable reduced GO (rGO) to be effectively used as an efficient charge carrier shuttle and a photocatalytic support material. So far, different approaches for this purpose, such as chemical reduction with reducing agents like hydrazine, hydrothermal reduction, and photochemical reduction using semiconductors, have been demonstrated [12]. Hydrazine and its derivatives have been proved the best GO reducing agents; however, owing to their toxicity, the search for alternate non-toxic compounds is still on. In the recent years, nanocrystalline semiconductor materials have attracted much attention because of their unique optical and electronic properties [13–15]. By controlling the particle size, the band gap of semiconductor nanoparticles can

*Corresponding author. Tel.: +81 29 8513354 4769.
E-mail address: FUKATA.Naoki@nims.go.jp (N. Fukata).

0272-8842/$ - see front matter © 2013 Elsevier Ltd and Techna Group S.r.l. All rights reserved.
http://dx.doi.org/10.1016/j.ceramint.2013.05.025

be tuned [16–18]. These nanoparticles exhibited enhanced properties when combined with graphene as a composite than as nanoparticles alone [19–21]. However, the aqueous insolubility of graphene restricts its practical application as a compositing host, whereas GO is very soluble due to its attached functional groups [22,23]. For this reason, one-pot synthesis of rGO-semiconductor nanoparticle composites from GO and other nanoparticles synthetic precursors is being actively researched. Nethravati et al. successfully synthesized graphene/metal sulfide nanocomposites, using H_2S as a sulfur source as well as reducing agent [24]. Cao et al. synthesized graphene/CdS nanocomposites through a solvothermal method for photocatalytic hydrogen production and optoelectronics [25]. Among semiconductors, CdS is one of the most important chalcogenide materials with a band gap lying in the visible region (2.42 eV at room temperature) [26], which finds use in many applications such as light emitting diodes (LEDs) [27], solar cells [28], photocatalysts [29], and optoelectronic devices [30]. Thermodynamically, CdS has a band potential suitable for a range of photocatalytic redox reaction, which can lead to greater usage of its good photocatalytic property. However, CdS nanoparticles have the limitations of rapid charge recombination of photoexcited electron-hole pairs, photocorrosion, and particle aggregation, all of which lead to an efficiency decrease of the photoinduced process. Nevertheless, when CdS is incorporated into graphene as a composite, the photoexcited electron–hole pair separation is facilitated and the charge recombination process retarded, and as a result, the overall photocatalytic activity is effectively enhanced [31].

In this paper, we report one-pot synthesis of CdS/rGO composites through an easy and simple wet chemical method, which, for the first time, uses thiourea as both a GO reducing agent and a sulfide precursor. Structural and morphological characterizations were done to show the efficiency of thiourea, and also to demonstrate the formation of CdS/rGO composite. To test the photocatalytic efficiency of the composite in comparison with CdS nanoparticles, we performed photocatalytic degradation of methyl orange (MO) under UV radiation. The composite showed a superior photocatalytic performance, reaching a 99% degradation of MO as compared to the 72% degradation exhibited by CdS nanoparticles.

2. Experimental

2.1. Synthesis of graphite oxide

Graphite oxide (GO) was synthesized from natural graphite powder following Hummer's method [32]. In this method, 2 g of graphite powder and 1 g of $NaNO_3$ were added to 46 mL of H_2SO_4 in an ice bath and under stirring. Then, 6 g of $KMnO_4$ was slowly added to the suspension, and the temperature was maintained below 10 °C. Subsequently, the resulting dark green suspension was removed from the ice bath, and its temperature increased to 35 °C, and maintained at that temperature for half an hour. Then, 92 mL of water was added to the mixture and its temperature was increased to 98 °C and maintained there for 2 h. The synthesis was finished by adding 280 mL of water and 30 mL of H_2O_2 (30%). Finally, the resulting brown colored mixture was washed with diluted HCl (10%), ethanol, and water, and then the mixture was dried in a vacuum oven for 12 h at 60 °C.

2.2. Synthesis of CdS/rGO composite

Cadmium acetate and thiourea [$SC(NH_2)_2$] were the chemicals used to synthesize CdS nanoparticles. One hundred milligram of graphite oxide powder was added to dehydrated ethanol, followed by ultrasonication for 1 h to obtain a homogeneous dispersion of GO. This GO dispersion was used for subsequent synthetic steps. 0.05 mol of cadmium acetate and 0.05 mol of thiourea were added to the GO dispersion under stirring. The reaction was performed at 60 °C for 4 h. The precipitate was washed and filtered with ethanol and water. This procedure was repeated three times. Then, filtered samples were dried in a vacuum oven at 60 °C for 12 h. Finally, the powders were calcined at 250 °C for 5 h.

2.3. Materials characterization

The crystalline structure of all the materials was investigated by powder X-ray diffraction (XRD) using a Rigaku Rintz Ultima diffractometer operating with CuKα radiation ($\lambda = 1.54056$ Å) and a scanning rate of 1 deg min^{-1}. The X-ray tube voltage and electric current were held at 40 kV and 40 mA, respectively. Raman spectra were obtained using a Horiba Jobin-Yvon spectrometer with a 514 nm (Green laser) excitation source, and the corresponding spectra were recorded from 100 cm^{-1} to 3000 cm^{-1}. The morphology and structure of the composite materials were examined through transmission electron microscopy (TEM) with a JEOL JEM 2100 microscope. A Fourier transform infrared (FTIR) study was performed using a Perkin-Elmer (spectrum 100 FTIR) spectrometer with KBr pellet-based samples in the frequency range from 4000 cm^{-1} to 400 cm^{-1}. Thermal properties of samples were analyzed by thermogravimetry (TG) measurements using SII EXSTAR 6000 with a TG/DTA6200 thermogravimetric analyzer from 40 °C to 1000 °C at a heating rate of 5 °C/min with sealed platinum pans under N_2 flow. Photoluminescence (PL) spectra were acquired using a Horiba Jobin-Yvon spectrometer with He–Cd laser. Element identification on the surface of the composites was analyzed by X-ray photoelectron spectroscopy (XPS), recorded on a Thermo Scientific Theta Probe spectrometer. The photocatalytic activity for the decomposition of MO was evaluated at room temperature in a cylindrical quartz reactor. The CdS nanoparticles and CdS/rGO composite were mixed with a MO aqueous solution (20 mg/L) in a 10:1 ratio. During irradiation of the quartz reactor by a UV lamp (SLUV-8, 365 nm) for desired time intervals, absorption spectra of the MO solution were monitored by a UV–vis–NIR spectrophotometer (model V-570).

3. Results and discussion

Fig. 1A shows the XRD patterns of GO, CdS and CdS/rGO composite. The XRD pattern of GO shows a major peak at 10.8° [33], corresponding to a (002) interplanar crystallographic spacing of 0.82 nm, which is much larger than that of natural graphite (0.335 nm) [34–36]. In the XRD patterns of CdS and CdS/rGO composite all the peaks could be indexed to the cubic phase of CdS nanoparticles (JCPDS no. 10-0454) [37]. The (002) diffraction peak of graphene was not properly resolved, as the same peak at ~25° overlapped with the (111) diffraction peak of CdS [38]. The primary size of the CdS nanoparticles is estimated to be 5 nm from the Debye–Scherrer equation.

To further investigate the CdS crystalline phase and rGO quality, Raman spectroscopy was employed as a powerful non-destructive tool to detect structural changes in GO during the wet chemical reaction process (Fig. 1B). Raman spectra of GO show the D band at 1358 cm^{-1} (breathing mode of *k*-point phonons with A_{1g} symmetry) and G band at 1595 cm^{-1} (first-order scattering of E_{2g} phonons). For CdS nanoparticles, the first, second, and third order longitudinal optical phonon modes (1LO, 2LO, and 3LO) are present at 300 cm^{-1}, 596 cm^{-1}, and 900 cm^{-1}, respectively. In the case of the CdS/rGO composite, rGO D and G bands appear at 1354 cm^{-1} and 1583 cm^{-1}, respectively. The D/G intensity ratio is larger in the composite material than in GO, which indicates the increase in the number of smaller sp^2 domains and a re-establishment of conjugated

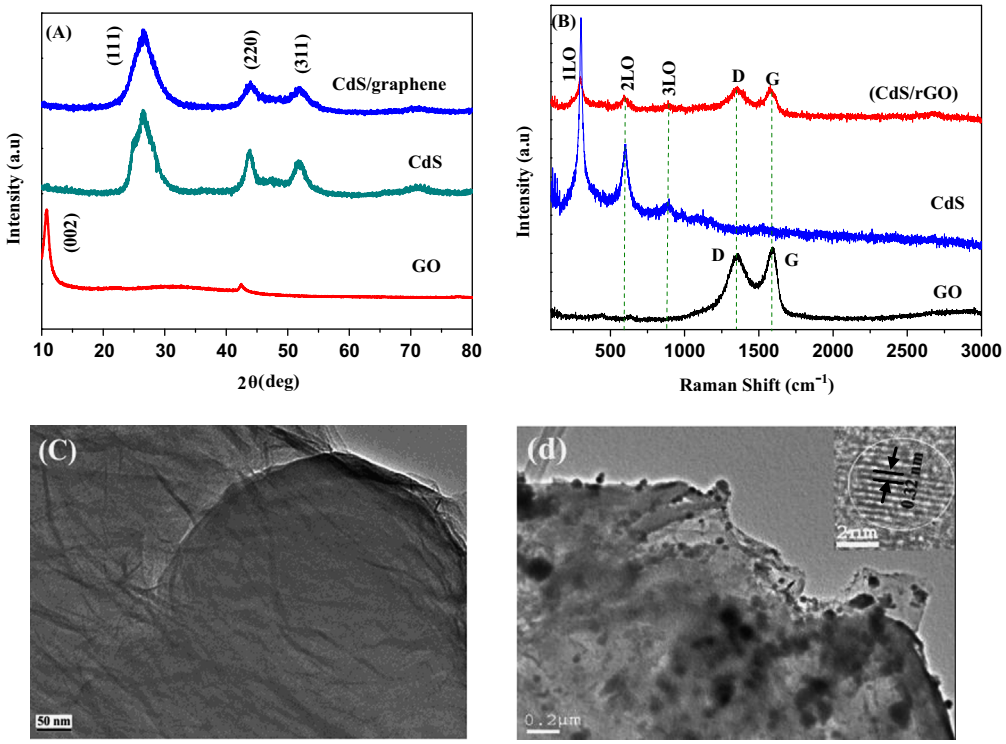

Fig. 1. (A) XRD patterns of GO, CdS nanoparticles and CdS/rGO composite. (B) Raman spectra of GO, CdS nanoparticles and CdS/rGO composite. TEM images of (C) GO and (D) CdS/rGO composite and inset shows the high resolution TEM image of CdS nanoparticle.

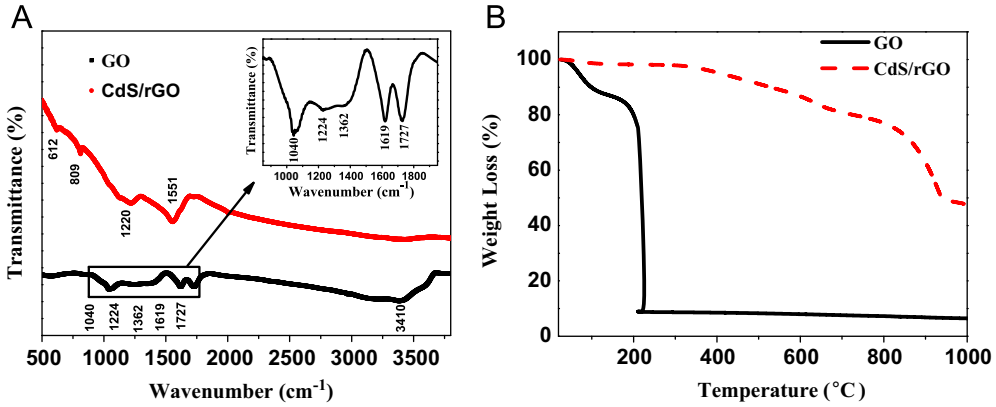

Fig. 2. (A) FTIR spectra of GO and CdS/rGO composite. Inset shows an FTIR spectrum of composite from 850 to 1950 cm^{-1}. (B) TG curve of GO and CdS/rGO composite.

graphene networks (rearomatization) [39]. In addition, in comparison with GO starting material, re-established graphene network size was smaller. This effect is able to increase the intensity ratio of D/G in CdS/rGO composite materials, in agreement with Pan et al. [40]. In the rGO Raman spectrum, an increase of the D/G intensity ratio is usually observed [41] suggesting a successful transformation of GO to rGO.

Fig. 1C and D shows the TEM images of GO and CdS/rGO composite, respectively. Fig. 1C shows the wrinkled structure of GO sheets. Fig. 1D shows that the CdS nanoparticles were deposited on the surface of the rGO. High resolution TEM (HRTEM) image (inset of Fig. 1D) of the nanoparticles shows lattice fringes with a 0.32 nm spacing in agreement with the (111) lattice plane of cubic CdS [42]. The CdS average particle size estimated from HRTEM images is 5 nm, which is consistent with the XRD results. From the above results we can conclude that GO is reduced to rGO during the synthesis because the amino group has the capability of reducing the functional group of GO, owing to the π–π interaction between the amino group of thiourea and functional groups of GO.

The formation of GO and CdS/rGO composite was characterized by FTIR spectroscopy (Fig. 2A). The FTIR spectra of GO shows a broad and strong peak at around 3395 cm^{-1} corresponding to the stretching vibrations of hydroxyl groups. Additional peaks appear at 1040 cm^{-1}, 1224 cm^{-1}, 1362 cm^{-1} and 1727 cm^{-1} that correspond to the C–O stretching, C–OH stretching, C–O–H bending and C═O stretching peaks of carboxyl groups, respectively. The vibrational peak of sp^2 hybridized C═C appears at 1619 cm^{-1}, which is assigned to skeletal vibrations of unoxidized graphitic domains [43]. In the case of the composite, some of the oxygen containing functional groups disappeared. The peak at 1551 cm^{-1} is attributed to the skeletal vibration of graphene sheets. This indicates the reduction of GO to rGO. The peaks at 612 cm^{-1} and 809 cm^{-1} correspond to the CdS nanoparticles [44]. These results provide an additional evidence for the formation of CdS/rGO composite.

Changes in the thermal stability and the composition of graphite oxide and CdS/rGO nanocomposite materials were analyzed by thermogravimetric analysis (TGA) under a nitrogen atmosphere (Fig. 2B). The weight loss of GO below 100 °C is a result of the evaporation of absorbed water and the major weight loss that occurs around 200 °C is assigned to the liable hydrophilic groups, yielding CO, CO_2 and steam, similarly with earlier reports [45,46]. Compared to GO, CdS/rGO composite shows much better thermal stability and gradual weight loss up to 800 °C. An abrupt weight loss in the range between 800 and 845 °C occurred due to the decomposition of CdS, in accordance with the thermal behavior of CdS/rGO [47].

The UV–vis–NIR absorption spectroscopy has been used to monitor the optical absorption behavior of the synthesized materials. The absorption spectra of GO, CdS nanoparticles and CdS/rGO are shown in Fig. 3A. GO exhibits an absorption feature at around 215 nm which corresponds to a π–π^* transition of C═C in GO and a shoulder around 320 nm due to n–π^* transitions of C═O [48]. Meanwhile, the CdS nanoparticles exhibit a strong absorption at wavelengths below 400 nm. In the absorption spectrum of CdS/rGO, the shoulder around 320 nm disappears due to the decrease in the concentration of carboxyl groups in rGO, and the absorption peak due to the π–π^* transition of C═C shifts to 248 nm [49]. The absorption of the CdS/rGO composite is higher than that of the CdS nanoparticles. These observations suggest that GO was reduced to rGO during the synthesis of the composite, and also imply the existence of coupling between CdS nanoparticles and rGO in the composite. Fig. 3B depicts the photoluminescence (PL) spectra of both pure CdS nanoparticles and CdS/rGO composite at the excitation wavelength of 325 nm. The PL spectrum of pure CdS nanoparticles shows a broad emission peak at 560 nm and a low intense emission peak at 422 nm [50]. The strong emission band centered at 560 nm might arise from the transition of trapped electrons on the surface states, which is due to interstitial sulfur lattice defects and sulfur vacancies of the CdS, to valence band of CdS nanoparticles [51]. Similarly, the low intense emission peak at 422 nm is due to the band edge emission of CdS nanoparticles. In the PL spectrum of the CdS/rGO composite, the intensity decreased for both the low intense band and broad emission bands in comparison with pure CdS nanoparticles. The decrease in PL intensity of the composite stems from the band alignment at the interface of CdS and rGO (inset of Fig. 3).

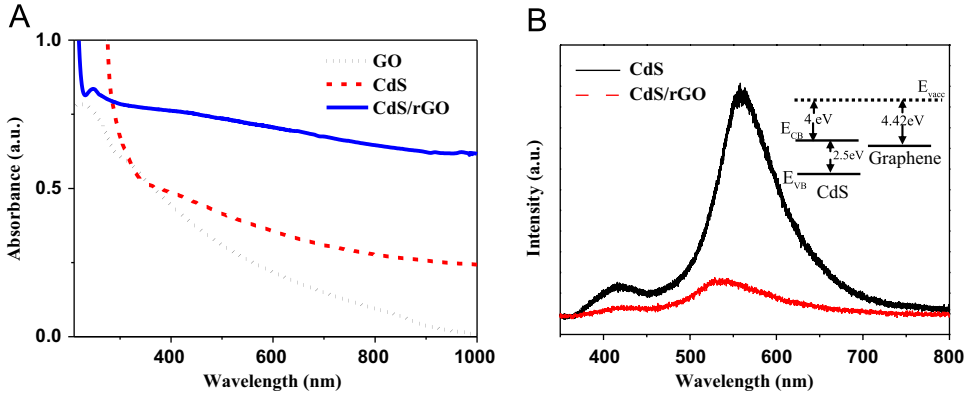

Fig. 3. (A) UV–vis–NIR absorption spectra of GO, CdS nanoparticles and CdS/rGO composite. (B) Photoluminescence spectrum of CdS nanoparticles and CdS/rGO composite. Inset shows the band alignment at the interface of CdS nanoparticles and rGO.

Since the electron affinity for CdS is χ_{CdS} = 4.00 eV and the Fermi level of the graphene is known to be 4.42 eV [30], direct electron transfer from the conduction band of photoexcited CdS nanoparticles to the rGO is therefore energetically favorable when CdS nanoparticles are attached to the rGO. Thus, the decrease in the intensity indicates the PL quenching appears due to the interaction between the surface of the CdS nanoparticles and rGO sheets [24].

To investigate the elemental composition and transformation of GO to rGO and CdS/rGO composite, we also carried out X-ray photoelectron spectroscopy (XPS) measurements (Fig. 4). Fig. 4A and B respectively shows the survey spectra of GO and CdS/rGO composite, which confirm the presence of C, O, Cd, and S. In the high resolution XPS spectrum of the C 1s peak of GO (Fig. 4C), a considerable degree of oxidation can be observed at peaks of 286.9 eV which can be assigned to the C–O and C–O–C oxygen containing groups [52]. In addition, the deconvoluted peak centered at 284.7 eV is attributed to the C–C, C = C, and C–H bonds (sp^2 hybridized). In contrast for the C 1s spectrum of the composite (Fig. 4D), the peak intensity from oxygen containing functional groups reduces substantially, confirming that GO has been converted to rGO. The high intense peak attributed to sp^2 of C = C bond. In addition, Fig. 5E shows the $Cd_{d5/2}$ and $Cd_{d3/2}$ core level peaks at 405.2 eV and 412.0 eV in the composite, which match well with the standard values of these peaks in CdS [53]. For the composite, the peak corresponding to S 2p core level is observed at 161.8 eV (Fig. 4F). This agrees well with its

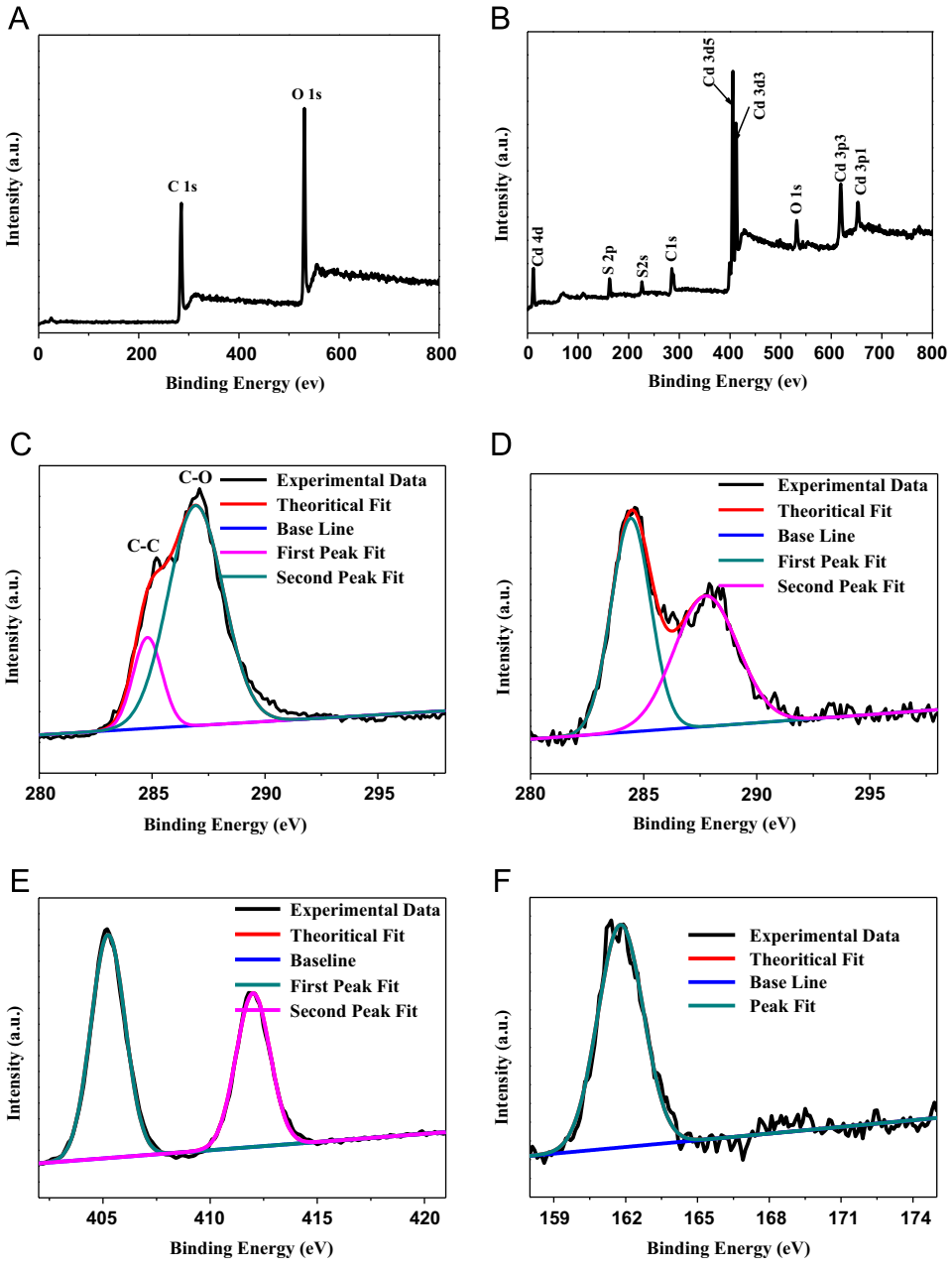

Fig. 4. (A and B) XPS survey spectrum of GO and CdS/rGO composite. (C and D) C 1s peak of GO and CdS/rGO composite. (E and F) Cd 3d and S 2p peak of CdS/rGO composite.

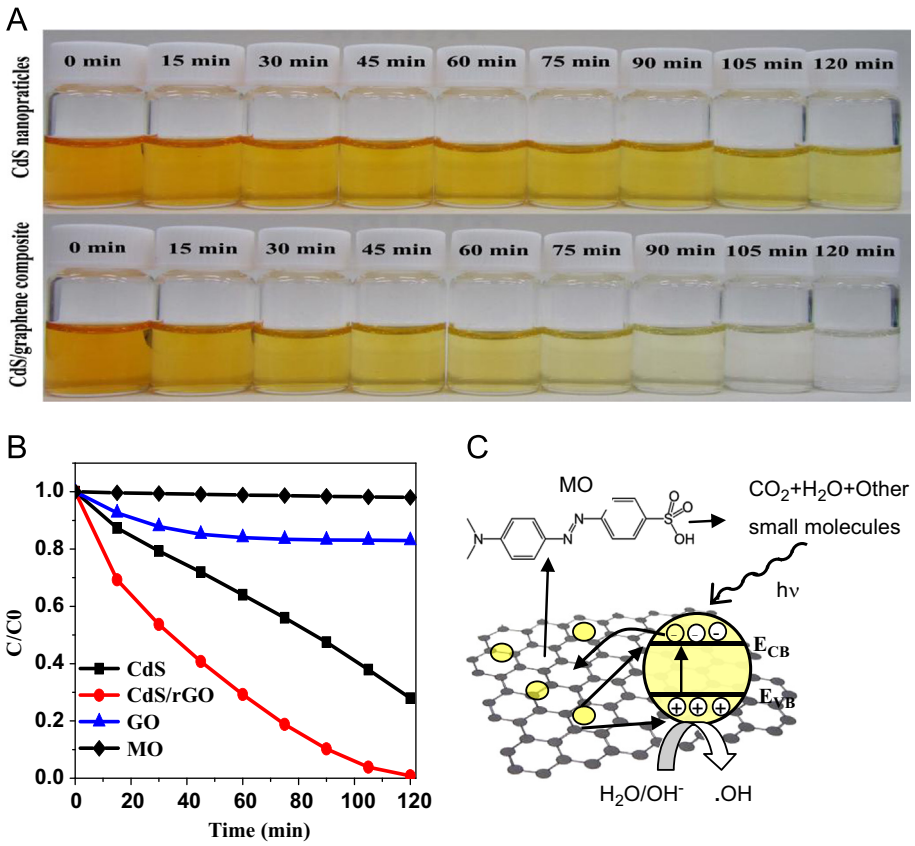

Fig. 5. (A) The optical photograph showing gradual color change of MO at different time intervals during the photodegradation process. (B) Degradation of MO, (C/C_0) as the function of irradiation time. (C) Scheme showing the charge transfers between rGO and CdS with photodegradation of MO molecules under UV light irradiation.

reported position [54,55]. These results clearly confirm the formation of CdS in the composite during the synthesis process and also the interaction of CdS with rGO.

To evaluate the photocatalytic activity of both CdS and CdS/rGO composites, the photodegradation of MO as a model organic pollutant was performed (Fig. 5). Fig. 5B shows the concentration changes of MO (C/C_0) as a function of UV irradiation time, where C_0 and C are its initial concentration and the concentration of MO after UV irradiation, respectively. Without any photocatalyst, only a 2% degradation within 2 h of UV irradiation was observed. However, in the presence of CdS nanoparticles, a photodegradation yield of 72% was obtained for the same irradiation time; similarly, the composite showed a 99% photodegradation yield. To understand clearly the enhancement of MO photodegradation by the composite, we also performed its photodegradation in the presence of only rGO while keeping all the other experimental conditions the same. This degradation study showed that nearly 17% of MO was degraded within 2 h of UV irradiation. Recent studies showed that GO can be used as a good photocatalytic degradation agent for organic pollutants [56]. In this case, from our FTIR study (Fig. 2A), it is clear that all the functional groups in GO are not fully removed during the reduction process. Thus, the degradation shown by rGO may be because of the presence of unreduced GO in the rGO sample that is responsible for ultrafast electron–hole recombination within the graphene network; hence, properly reduced GO parts did not show any significant photodegradation [57]. The photocatalytic activity mainly depends on the number of available photo-electrons of the photocatalyst, and also on the surface area of the catalyst where the photodegradation occurs. In the case of CdS nanoparticles, photogenerated electrons reach the surface and start the photodegradation reaction. Faster electron–hole recombination in CdS leads to a delay in the degradation process. However, when CdS nanoparticles are attached to graphene sheets, the photoelectrons quickly transfer to rGO, thus facilitating the electron–hole separation (Fig. 5C); in addition, the increased surface area of graphene sheets accelerates the MO photodegradation. The OH^- present in aqueous solution takes the holes from CdS to form hydroxyl radicals ($\cdot OH$), which also has a high oxidation potential for the oxidation of organic dye molecules as suggested by Wang et al. [58].

4. Conclusions

In this work, we demonstrated the synthesis of CdS/rGO nanocomposites through an easy wet chemical method, using thiourea, which acted as both a sulfur source and a reducing agent. XRD showed CdS nanoparticles had crystallized in a cubic phase and their primary particle size as calculated by the Debye–Scherrer equation was 5 nm. FTIR and Raman spectra showed the successful transformation of GO to rGO.

In addition, XPS demonstrated the deoxygenation of the surface of the composite. TEM images showed the CdS nanoparticles had deposited on the surface of the rGO sheets. TG curves showed the composite material had good thermal stability compared to GO. Finally, the photoluminescence (PL) spectra of pure CdS and CdS/rGO showed two emission peaks. In the composite material, the luminescence quenching revealed a high efficiency of charge transfer between the surface of the rGO and CdS nanoparticles, which could be useful in new optoelectronic and photovoltaic devices. The photodegradation of MO showed the success of using CdS/rGO composites in the photoinduced detoxification of organic wastes.

Acknowledgment

The authors are very much thankful to the National Institute for Material Science (NIMS), Japan for providing the facilities to do the characterization. This work was supported by a Funding Program for Next Generation World-Leading Researchers (NEXT Program)

References

[1] H.L. Guo, X.F. Wang, Q.Y. Qian, F.B. Wang, X.H. Xia, A green approach to the synthesis of graphene nanosheets, ACS Nano 3 (2009) 2653–2659.
[2] Y. Zhou, Q. Bao, L.A.L. Tang, Y. Zhong, K.P. Loh, Hydrothermal dehydration for the green reduction of exfoliated graphene oxide to graphene and demonstration of tunable optical limiting properties, Chemistry of Materials 21 (2009) 2950–2959.
[3] F. Liu, S. Song, D. Xue, H. Zhang, Folded structured graphene paper for high performance electrode materials, Advanced Materials 24 (2012) 1089–1094.
[4] D. Li, M.B. Muller, S. Gilje, R.B Kaner, G.G. Wallace, Processable aqueous dispersions of graphene nanosheets, Nature Nanotechnology 3 (2008) 101–105.
[5] P. Avouris, Z. Chen, V. Perebeinos, Carbon-based electronics, Nature Nanotechnology 2 (2007) 605–615.
[6] C.H. Xu, X.B. Wang, J.C. Wang, H.T. Hu, Synthesis and photoelectrical properties of b-cyclodextrin functionalized graphene materials with high bio-recognition capability, Chemical Physics Letters 498 (2010) 162–167.
[7] X. Wang, L.J. Zhi, K. Mullen, Transparent, conductive graphene electrodes for dye-sensitized solar cells, Nano Letters 8 (2008) 323–327.
[8] S. Stankovich, D.A. Dikin, G.H.B. Dommett, K.A. Kohlhaas, E.J. Zimney, E.A. Stach, Graphene-based composite materials, Nature 442 (2006) 282–286.
[9] S.R.C. Vivekchand, C.S. Rout, K.S. Subrahmanyam, A. Govindaraj, C.N.R. Rao, Graphene-based electrochemical supercapacitors, Journal of Chemical Sciences 120 (2008) 9–13.
[10] T. Szabo, E. Tombacz, E. Illes, I. Dekany, Enhanced acidity and pH-dependent surface charge characterization of successively oxidized graphite oxides, Carbon 44 (2006) 537–545.
[11] N.A. Kotov, I. Dekany, J.H. Fendler, Ultrathin graphite oxide–polyelectrolyte composites prepared by self-assembly: transition between conductive and non-conductive states, Advanced Materials 8 (1996) 637–641.
[12] X. Pan, Y. Zhao, S. Liu, C.L. Korzeniewski, S. Wang, Zhaoyang Fan, Comparing graphene–TiO_2 nanowire and graphene–TiO_2 nanoparticle composite photocatalysts, ACS Applied Materials & Interfaces 4 (2012) 3944–3950.
[13] A.P. Alivisatos, Semiconductor clusters, nanocrystals, and quantum dots, Science 271 (1996) 933–937.
[14] C. Zhang, K. Li, S. Song, D. Xue, Two-phase route to high quality ZnO quantum dots with high stability of dispersity, structure and optical properties, Science of Advanced Materials 4 (2012) 1148–1153.
[15] H. Xia, D. Xue, L. Lu, Double-shelled nanocapsules of V2O5-based composites as high-performance anode and cathode materials for Li ion batteries, Journal of the American Chemical Society 131 (2009) 12086–12087.
[16] C.B. Murray, D.J. Norris, M.G. Bawendi, Synthesis and characterization of nearly monodisperse CdE (E=sulfur, selenium, tellurium) semiconductor nanocrystallites, Journal of the American Chemical Society 115 (1993) 8706–8715.
[17] C. Sun, D. Xue, Tailoring anisotropic morphology at the nanoregime: surface bonding motif determines the morphology transformation of ZnO nanostructures, Journal of Physical Chemistry C 117 (2013) 5505–5511.
[18] K. Li, Y. Li, D. Xue, Band gap engineering of crystal materials: band gap estimation of semiconductors via electronegativity, Functional Materials Letters 05 (2012) 1260002.
[19] P. Lu, D. Xue, MoO_2/reduced graphene oxide composite electrode with improved cycling performance and high capacitance for supercapacitors, Journal of Nanoengineering and Nanomanufacturing 3 (2013) 73–78.
[20] F. Liu, J. Liu, D. Xue, CoO/graphene composite for high performance Li-ion battery anode, Materials Focus 1 (2012) 160–163.
[21] K. Chen, J. Liu, D. Xue, Synthesis of Cu_2O nanocrystals and Cu_2O/graphene composite paper for lithium-ion battery anode materials, Energy and Environment Focus 1 (2012) 50–56.
[22] P. Lu, D. Xue, MoO_2 nanocrystals decorated reduced graphene oxide sheets as high capacity electrode for supercapacitor applications, Journal of Nanoengineering and Nanomanufacturing 2 (2012) 332–338.
[23] F. Liu, D. Xue, Flexible composite electrodes upon aerogel derived graphene paper towards lithium-ion batteries, Energy and Environment Focus 1 (2012) 93–98.
[24] C. Nethravathi, T. Nisha, N. Ravishankar, C. Shivakumara, M. Rajamathi, Graphene–nanocrystalline metal sulphide composites produced by a one-pot reaction starting from graphite oxide, Carbon 47 (2009) 2054–2059.
[25] A.N. Cao, Z. Liu, S.S. Chu, M.H. Wu, Z.M. Ye, Z. Cai, Y.L. Chang, S.F. Wang, Q.H. Gong, Y.F. Liu, A facile one-step method to produce graphene–CdS quantum dot nanocomposites as promising optoelectronic materials, Advanced Materials 22 (2010) 103–106.
[26] T. Thongtem, A. Phuruangrat, S. Thongtem, Solvothermal synthesis of CdS nanowires templated by polyethylene glycol, Ceramics International 35 (2009) 2817–2822.
[27] Q. Zhang, Y. Gao, S. Zhang, J. Wu, H. Zhou, J. Yang, X. Tao, Y. Tian, Photophysical properties of spherical aggregations of CdS nanocrystals capped with a chromophoric surface agent, Dalton Transactions 41 (2012) 7067–7072.
[28] H. Li, M. Eastman, R. Schaller, W. Hudson, J. Jiao, Hydrothermal synthesis of CdS nanoparticle-decorated TiO_2 nanobelts for solar cell, Journal for Nanoscience and Nanotechnology (2011) 8517–8521.
[29] J. Nayak, S.N. Sahu, J. Kasuya, S. Nozaki, CdS–ZnO composite nanorods: synthesis, characterization and application for photocatalytic degradation of 3,4-dihydroxy benzoic acid, Applied Surface Science 254 (2008) 7215–7218.
[30] B.T. Raut, M.A. Chougule, Shashwati Sen, R.C. Pawar, C.S. Lee, V.B. Patil, Novel method of fabrication of polyaniline–CdS nanocomposites: structural, morphological and optoelectronic properties, Ceramics International 38 (2012) 3999–4007.
[31] L. Han, P. Wang, S. Dong, Progress in graphene-based photoactive nanocomposites as a promising class of photocatalyst, Nanoscale 4 (2012) 5814–5825.
[32] W.S. Hummers, R.E. Offeman, Preparation of graphitic oxide, Journal of the American Chemical Society 80 (1958) 1339-1339.
[33] P.S. Teoa, H.N. Limb, N.M. Huanga, C.H. Chiac, I. Harrison, Room temperature in situ chemical synthesis of Fe_3O_4/graphene, Ceramics International 38 (2012) 6411–6416.

[34] L. Jia, D.H. Wang, Y.X. Huang, A.W. Xu, H.Q. Yu, Highly durable N-doped graphene/CdS nanocomposites with enhanced photocatalytic hydrogen evolution from water under visible light irradiation, Journal of Physical Chemistry C 115 (2011) 11466–11473.
[35] J. Wu, X. Shen, L. Jiang, K. Wang, K. Chen, Solvothermal synthesis and characterization of sandwich-like graphene/ZnO nanocomposites, Applied Surface Science 256 (2010) 2826–2830.
[36] H. Bai, Y. Xu, L. Zhao, C. Li, G. Shi, Non-covalent functionalization of graphene sheets by sulfonated polyaniline, Chemical Communications (2009) 1667–1669.
[37] F. Chen, Y. Cao, D. Jian, X. Niu, Facile synthesis of CdS nanoparticles photocatalyst with high performance, Ceramics International 39 (2013) 1511–1517.
[38] J.S. Chen, Z. Wang, X.C. Dong, P. Chen, X.W. (David) Lou, Graphene-wrapped TiO_2 hollow structures with enhanced lithium storage capabilities, Nanoscale 3 (2011) 2158–2161.
[39] S. Song, W. Gao, X. Wang, X. Li, D. Liu, Y. Xing, H. Zhang, Microwave-assisted synthesis of BiOBr/graphene nanocomposites and their enhanced photocatalytic activity, Dalton Transactions 41 (2012) 10472–11076.
[40] S. Pan, X. Liu, ZnS–graphene nanocomposite: synthesis, characterization and optical properties, Journal of Solid State Chemistry 191 (2012) 51–56.
[41] K.N. Kudin, B. Ozbas, H.C. Schniepp, R.K. Prud'homme, I.A. Aksay, R. Car, Raman spectra of graphite oxide and functionalized graphene Sheets, Nano Letters 8 (2007) 36–41.
[42] P.S. Chowdhury, P. Sen, A. Patra, Optical properties of CdS nanoparticles and the energy transfer from CdS nanoparticles to Rhodamine 6G, Chemical Physics Letters 413 (2005) 311–314.
[43] Y.X. Xu, H. Bai, G.W. Lu, C. Li, G.Q. Shi, Flexible graphene films via the filtration of water-soluble noncovalent functionalized graphene sheets, Journal of the American Chemical Society 130 (2008) 5856–5857.
[44] S. Stankovich, D.A. Dikin, R.D. Piner, Synthesis of graphene-based nanosheets via chemical reduction of exfoliated graphite oxide, Carbon 45 (2007) 1558–1565.
[45] B.T. Raut, M.A. Chougule, S.R. Nalage, D.S. Dalavi, S. Mali, P.S. Patil, V.B. Patil, CSA doped polyaniline/CdS organic–inorganic nanohybrid: physical and gas sensing properties, Ceramics International 38 (2012) 5501–5506.
[46] H. Feng, R. Cheng, X. Zhao, X. Duan, J. Li, A low-temperature method to produce highly reduced graphene oxide, Nature Communications 4 (2013) 1539.
[47] D. Pathania, Sarita, B.S. Rathore, Synthesis, characterization and photocatalytic application of bovine serum albumin capped cadmium sulphide nanoparticles, Chalcogenide Letters 8 (2011) 396–404.
[48] G. Eda, Y.-Y. Lin, C. Mattevi, H. Yamaguchi, H.-A. Chen, I.-S. Chen, C.-W. Chen, M. Chhowalla, Blue photoluminescence from chemically derived graphene oxide, Advanced Materials 22 (2010) 505–509.
[49] J. Wua, S. Baia, X. Shena, L. Jiang, Preparation and characterization of graphene/CdS nanocomposites, Applied Surface Science 257 (2010) 747–751.
[50] J. Cheng, S. Wang, X.Y. Li, Y. Yan, S. Yang, C.L. Yang, J.N. Wang, W.K. Ge, Fast interfacial charge separation in chemically hybridized CdS–PVK nanocomposites studied by photoluminescence and photoconductivity measurements, Chemical Physics Letters 333 (2001) 375–380.
[51] R.M. Nirmal, K. Pandian, K. Sivakumar, Cadmium (II) pyrrolidine dithiocarbamate complex as single source precursor for the preparation of CdS nanocrystals by microwave irradiation and conventional heating process, Applied Surface Science 257 (2011) 2745–2751.
[52] X.-L. Wu, L. Wang, C.-L. Chen, A.-W. Xuc, X.-K. Wang, Water-dispersible magnetite-graphene-LDH composites for efficient arsenate removal, Journal of Materials Chemistry 21 (2011) 17353–17359.
[53] C.D. Wanger, W.M. Riggs, L.E. Davis, J.F. Moulder, G.E.Muilenberg, Handbook of X-ray Photoelectron Spectroscopy, Perkin-Elmer Corp., Physical Electronics Division, Eden Prairie, Minnesota, USA, 1979, pp. 114.
[54] U. Winkler, D. Eich, Z.H. Chen, R. Fink, S.K. Kulkarni, E. Umbach, Thermal behaviour of CdS nanoparticles investigated by high resolution photoelectron spectroscopy, Physica Status Solidi A 173 (1999) 253–259.
[55] P.K. Narayanam, G. Singh, V.D. Botcha, D.S. Sutar, S.S. Talwar, R.S. Srinivasa, S.S. Major, Growth of CdS nanocrystallites on graphene oxide Langmuir–Blodgett monolayers, Nanotechnology 23 (2012) 325605.
[56] K. Krishnamoorthy, R. Mohan, S.-J. Kim, Graphene oxide as a photocatalytic material, Applied Physics Letters 98 (2011) 244101–244103.
[57] F. Xia, T. Mueller, Y.-M. Lin, A. Valdes-Garcia, P. Avouris, Ultrafast graphene photodetector, Nature Nanotechnology 4 (2009) 839–843.
[58] X. Wang, H. Tian, Y. Yang, H. Wang, S. Wang, W. Zheng, Y. Liu, Reduced graphene oxide/CdS for efficiently photocatalystic degradation of methylene blue, Journal of Alloys and Compounds 524 (2012) 5–12.